Journal of Cultural Heritage 73 (2025) 1–10

Contents lists available at ScienceDirect

Journal of Cultural Heritage

journal homepage: www.elsevier.com/locate/culher

Original article

XMapsLab: A program for the creation and study of maps for Cultural Heritage

Domingo Martín[a,1,*], Germán Arroyo[a], Juan Ruiz de Miras[a], Luis López[a], María Rosario Blanc[b], José Luis Vílchez[b], Philippe Sarrazin[c], Juan Carlos Torres[a]

[a] *Department of Software Engineering, University of Granada, Spain*
[b] *Department of Analytical Chemistry, University of Granada, Spain*
[c] *eXaminart, California, USA*

ARTICLE INFO

Article history:
Received 11 March 2024
Accepted 14 February 2025

Keywords:
XRF mapping
Interpolation
Data analysis
Painting study
GPU programming

ABSTRACT

The creation of maps through the application of techniques such as X-Ray Fluorescence (XRF), X-Ray Diffraction (XRD), Raman spectroscopy, multispectral analysis, ultraviolet (UV), and infrared (IR) radiation has become critical in the domain of Cultural Heritage for the analysis of materials. Limitations in data acquisition, particularly with more cost-effective and accessible devices, often restrict measurements to a sparse number of locations. This necessitates the employment of interpolation methods to extrapolate values for the unmeasured positions within the image. This paper introduces XMapsLab a software solution designed to facilitate the generation and examination of maps. XMapsLab utilizes GPU-optimized versions of interpolation methods, achieving speed enhancements ranging from one to two orders of magnitude. Such improvements markedly expand the capabilities of professionals to engage with and analyze data in real-time. Additionally, the software incorporates various interpolation methods, enhancing the robustness of the results and bolstering the confidence of experts in their conclusions. The real-time functionality of XMapsLab enables the development of new procedures for exploring hypotheses regarding the presence and distribution of pigments. This includes the integration of boolean and numerical operations for map combination, allowing users to investigate hypotheses and conditions in a direct, potent, and intuitive manner. The software developed is freely available and open-source, underscoring our commitment to supporting the broader Cultural Heritage community.

1. Introduction

Maps, as representations of the values of physical phenomena or models not directly related to visible information, have emerged as indispensable tools for experts seeking to understand these phenomena. Examples of such maps include those depicting temperature, atmospheric pressure, or rainfall levels in a specified area.

Within the domain of chemical applications, especially in Cultural Heritage, the generation of maps using data derived from various techniques—such as X-Ray Fluorescence (XRF) [1], X-Ray Diffraction (XRD)) [2], multispectral imaging [3–6], Raman spectroscopy [7], ultraviolet (UV) and infrared (IR) radiation [8], among others—has become pivotal for material analysis [9–22]. The spatial analysis of chemical elements and pigments in artworks offers profound insights into aspects such as their authenticity, historical period of creation, processes of restoration, and the uncovering of concealed drawings in underlying layers. An exemplification of a map is presented in Fig. 1.

Currently, the production of maps is facilitated by computer programs. In the field of material studies in Cultural Heritage, it is commonplace for researchers to devise specialized solutions for distinct challenges, which may not be readily applicable to other contexts. A notable challenge arises when interpolation is required to compute values for unmeasured positions across the entirety of an image. To address this, a singular, generic method, which notably integrates color information—providing a significant enhancement over traditional interpolation techniques—is employed to correlate the resulting maps closely with the depicted elements or motifs within paintings and other artworks, thereby aiding ex-

* Corresponding author.
E-mail addresses: dmartin@ugr.es (D. Martín), arroyo@ugr.es (G. Arroyo), dmiras@ugr.es (J. Ruiz de Miras), luislopez@ugr.es (L. López), mrblanc@ugr.es (M.R. Blanc), jvilchez@ugr.es (J.L. Vílchez), philippe.sarrazin@examinart.com (P. Sarrazin), jctorres@ugr.es (J.C. Torres).
[1] Present address: Department of Software Engeneering, Escuela Técnica de Ingeniería Informática y Telecomunicación, Calle Periodista Daniel Saucedo Aranda s/n 18014 Granada.

https://doi.org/10.1016/j.culher.2025.02.011

Fig. 1. Example of a map of potassium (K) obtained with MHD method with a discrete palette of 5 intervals using "The Transfiguration" example.

perts in the interpretation of pigment distribution. This method, developed by Martín-Ramos and Chiari [23], herein referred to as MHD [24], is described in detail in their publication. Nonetheless, its practical application is largely confined to the *SmART_scan* program, which has been used in several research endeavors [25–28]. A critical limitation of this method, however, is its computational inefficiency with standard-sized images, often necessitating the use of smaller images or enduring extended processing times.

It is crucial to acknowledge that while recent articles exploring the use of Artificial Intelligence (AI), particularly convolutional neural networks (CNN) [29–31], for pigment identification in paintings may appear to offer a parallel solution, their objectives and outcomes differ significantly from our approach. Despite their innovative approach, these classification algorithms are not suited for generating maps that detail the quantities of chemical elements present, as they assign a singular label to each pigment identified in a given point.

In response to these challenges, this article introduces XMapsLab a comprehensive software suite engineered for map generation through interpolation, with a particular emphasis on applications involving XRF and XRD data. XMapsLab boasts several key features:

- Implementation of the Martín-Ramos and Chiari [23] interpolation method, optimized for GPU processing. This optimized implementation has demonstrated speed enhancements ranging from one to two orders of magnitude compared to traditional CPU-based processing, significantly augmenting the efficiency with which experts can process and analyze data in real time.
- Inclusion of additional interpolation techniques, notably the Radial Basis Function method, which may be utilized independently or in conjunction with the MHD method to circumvent its limitations and corroborate the accuracy of the results [24].
- The development of a supplementary tool, Laboratory, enables experts to explore various hypotheses concerning the presence or absence of pigments through the analysis of element distributions. This tool facilitates the combination of maps via logical and arithmetic operations through an intuitive block editor interface.
- The software is freely available and open-source, ensuring broad accessibility and compatibility across Windows and Linux operating systems.

2. Research aim

The purpose of this work is to unveil a novel software tool aimed at enhancing material analysis within Cultural Heritage research. A prevalent approach in material studies involves generating maps to visualize the spatial distribution of chemical elements, derived from measurement data obtained through methods such as X-Ray Fluorescence (XRF). Typically, this process necessitates the application of interpolation techniques due to the limited number of measurements produced by commonly used devices.

The innovation of our work lies in implementation of several interpolation methods, including the most used one, Minimum Hypercube Distance (MHD), using Graphics Processing Unit (GPU) technology. The use of several methods address the limitations inherent to all them, enhancing the robustness of the results. This new implementation delivers a substantial increase in processing speed, achieving enhancements of up to two orders of magnitude over existing methods. This improvement facilitates real-time analysis, contrasting sharply with the protracted durations previously required for obtaining results.

This advancement significantly broadens the analytical possibilities, enabling the formulation and exploration of hypotheses regarding the presence of pigments through the real-time combination of elemental maps (XRF) with Boolean and numerical operations mimicking the capabilities of an XRD device to a certain extent.

3. Material and methods

XMapsLab is a program meticulously crafted for professionals in the Cultural Heritage domain, with a particular focus on those conducting material analyses through X-Ray Fluorescence (XRF) and X-Ray Diffraction (XRD) techniques. Its core functionality enables the generation of maps by employing data mapping functions on values obtained from specified locations (see Section 5). A significant benefit of this software is its capability to produce maps in real time, eliminating the extended waiting periods traditionally associated with such processes. Moreover, the integration of a feature for analyzing map combinations enhances its utility by facilitating the determination of pigment presence or absence. Prior to exploring the specific methods and their technical execution, it is imperative to outline the contextual backdrop against which map generation occurs.

3.1. Maps definition

Maps are pivotal tools in converting various information types into visual data for intuitive human interpretation. Historically used for representing temperature variations and weather patterns, their application extends to material science for visualizing chemical element and pigment distributions in artworks, facilitating enhanced analysis. Map creation involves two key processes: generating values and assigning colors to these values, typically using the RGB color model to map real numbers to specific color combinations.

The necessity for interpolation arises from the measurement techniques' limitations, where some devices capture extensive data points rapidly, while others, like XRF and XRD devices, are constrained to slower, single-sample measurements. This disparity necessitates interpolation, particularly when data is sparse compared to the desired image resolution.

Integrating high-resolution photographic data, often containing millions of pixels, with elements or pigment maps from limited measurements poses significant challenges. For example, fifty measurements from a handheld XRF spectrometer represent a fraction of the data required for a detailed map, underscoring interpolation's critical role in achieving comprehensive material composition representation across an artwork.

This context sets the stage for discussing the significance, applications, and challenges of interpolation methods in map creation, emphasizing their contribution to bridging the gap between limited measurements and the need for detailed artwork analysis.

3.2. Interpolation methods for maps

The accuracy of interpolation methods in generating maps that represent real data is contingent upon the volume of information captured and the inherent characteristics of the interpolation technique employed. It is critical to acknowledge that some methods may precisely model the phenomenon under analysis, demonstrating proficiency in capturing either gradual or abrupt transitions, whereas others might not achieve the same level of accuracy. Consequently, experts utilizing these maps must be cognizant of the limitations inherent to the information obtained through these methods.

In its current iteration, XMapsLab incorporates two principal interpolation methods: the Minimum Hypercube Distance (MHD) and the Radial Basis Function (RBF), as advocated by [24]. The MHD method is favored for its robust performance, adeptly handling both gradual and sharp variations commonly observed in artworks. Conversely, the RBF method, while effective in interpolating values, is predominantly suited for scenarios characterized by smooth transitions. The outcomes derived from the RBF method can serve as supplementary data, potentially corroborating or questioning the conclusions drawn from the MHD method.

It is imperative to emphasize that the application of these interpolation methods is exclusively based on the measured values specific to each element or pigment. For instance, in constructing a map to represent iron (Fe), only the data pertaining to Fe measurements are utilized, disregarding information related to other elements such as lead (Pb) or sulfur (S).

3.2.1. Minimum Hypercube Distance (MHD)

This interpolation technique, tailored specifically for the fields of chemistry and materials analysis within Cultural Heritage contexts [23], presents a notable innovation through its incorporation of color information in the interpolation process. This advancement distinguishes it from conventional methods that rely solely on quantitative measurements. The color-based approach of MHD facilitates the accurate portrayal of both gradual transitions and distinct discontinuities observed in artworks, enabling it to depict the juxtaposition of varying pigments with remarkable precision. For instance, it adeptly identifies regions where distinct pigments, such as a red pigment adjacent to a contrasting pigment, are applied in close proximity, thereby reflecting the intricate use of color in historical artifacts.

The operational principle of MHD is grounded in the calculation of the minimum distance between a target pixel, whose element or pigment value is unknown, and the nearest measured pixel with known position, color, and value. This methodology ensures that the selected pixel with the closest color and spatial proximity is used as a reference for the unmeasured pixel, thereby attributing a corresponding value. Such a correlation between the interpolated values and the actual coloration seen in the artwork allows for an enhanced alignment with the visual characteristics of the subject, aiding experts in distinguishing between various regions with greater ease.

Despite its efficacy, it is imperative to acknowledge the potential for inaccuracies in the MHD method, particularly in instances where measurement data are sparse or absent, leading to extrapolations that may not fully align with underlying layers not visible on the surface. This method, integral to the functionality of the *SmART_scan* program, has been instrumental in advancing the analysis of Cultural Heritage materials by providing insights into the compositional variance across artworks.

Fig. 2 exemplifies the outcomes achievable through the application of the MHD method, showcasing its capacity to elucidate the complex interplay of colors and pigments in historical pieces.

3.2.2. Radial Basis Function (RBF)

In their investigative study, Martín et al. [24] scrutinized the efficacy and precision of various interpolation techniques in the context of map creation. A pivotal insight from this research is the realization that while certain interpolation methods offer reliable outcomes, absolute accuracy in reflecting real data may not always be attainable. Consequently, the researchers advocate for a multifaceted approach in evaluating results, suggesting the integration of multiple interpolation methods to substantiate the findings. The Minimum Hypercube Distance (MHD) method serves as the foundational technique, complemented by other methods, notably the

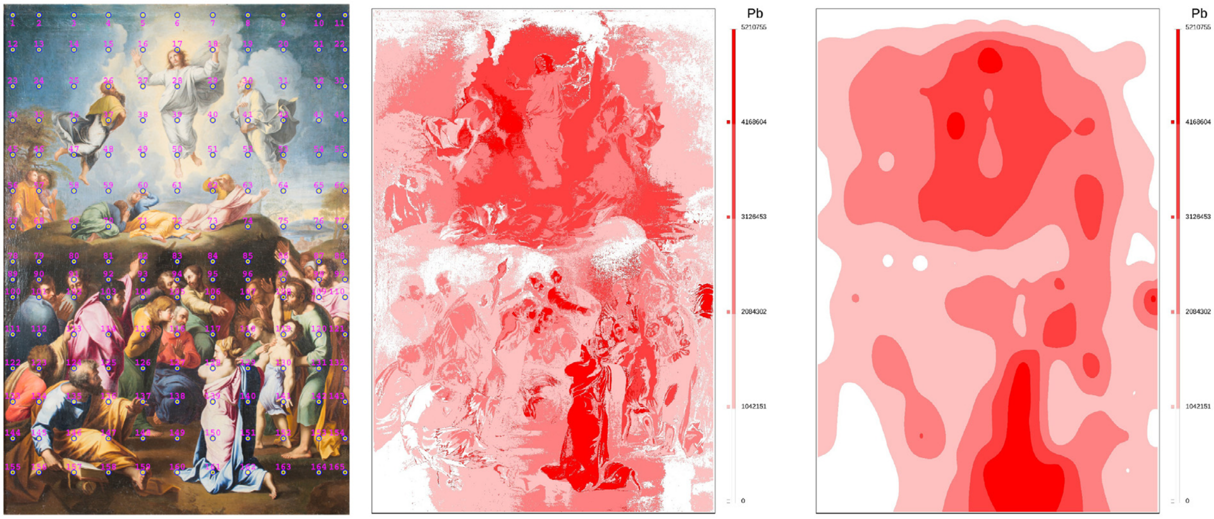

(a) "The Transfiguration" (b) Lead (Pb) MHD (c) Lead (Pb) RBF Linear

Fig. 2. Examples of interpolation maps. We have data for "The Transfiguration," including the original image with measurement positions and maps obtained using MDH and RBF methods. The input image has dimensions of 3020 pixels x 4456 pixels (W × H), with a total of 165 measurement positions.

Radial Basis Function (RBF) [32] and Kriging) [33], due to their analytical reliability and computational feasibility. Among these, the RBF method, characterized by its computational simplicity, was selected for implementation in XMapsLab.

The RBF interpolation strategy is delineated by its utilization of a composite of basis functions, each modulated by specific weights or factors—a methodology paralleled in Kriging and Barnes algorithms. This entails the strategic placement of basis functions at measured data points across the domain of interest, with these functions potentially extending across the entire analysis area. The radial symmetry intrinsic to RBF, exemplified by Gaussian functions, allows for the evaluation of distances from a central point, thereby facilitating the aggregation of weighted basis function values to deduce the interpolated value at any given location. The determination of appropriate weights through a system of equations is crucial to this process.

In the realm of painting analysis, RBF and analogous conventional interpolation methods present both merits and limitations. Their established validity and broad application underscore their utility. However, a notable limitation arises from their inherent tendency to model data transitions smoothly, which may not accurately reflect the discrete or abrupt changes indicative of different pigments or artistic techniques, especially in instances where color variations are minimal or non-existent.

Fig. 2 illustrates the type of results attainable through the RBF method, highlighting its capacity to delineate gradual transitions in data values, albeit with the noted limitation regarding the depiction of sharp demarcations.

3.3. Contours image

To overcome the Radial Basis Function (RBF) method's limitations in capturing the complex shapes within artworks, an enhancement involving contour image generation from the original artwork has been introduced. This addition improves the visualization of element distributions, making the maps more informative for expert analysis.

The contour extraction leverages the Difference of Gaussians (DoG) algorithm [34], noted for its programming simplicity, computational speed, and effectiveness. This method provides varied results, offering a detailed view of the artwork's structural nuances.

The comparison of maps using both MHD and RBF methods shows the MHD's superior alignment with the artwork's physical shapes (see Fig. 3). In contrast, the RBF method, despite accurately indicating maxima locations, tends to produce smoother interpolations that may not as precisely mirror the artwork's intricacies. The inclusion of contour overlays enhances the analytical value of the RBF-generated maps, enabling a deeper interpretive analysis and improved reliability of results. However, discrepancies between the two methods' maps necessitate expert scrutiny for accurate data interpretation. This can be facilitated with the computation of discrepancies between maps generated by the two methods (refer to Fig. 3d)

3.4. Laboratory

Laboratory is a module engineered to enable the representation of hypotheses regarding pigment presence, guided by the spatial distribution and intensity values of elements. This is achieved through a suite of operations tailored to the specific requirements of each hypothesis. For example, identifying potential areas of cinnabar involves checking for simultaneous Hg and S presence, thereby generating a new map that highlights these locations. Initially, continuous values are transformed into binary values through the application of a predefined threshold. Subsequently, these binary values are subjected to a logical operation for combination purposes. In the context of detecting cinnabar, an AND operation is employed. This operation yields a true value exclusively when both input values are true; in all other instances, a false value is generated. Beyond binary operations, continuous value operations offer a nuanced approach to mapping pigment presence. For instance, calculating the geometric mean of Hg and S intensities ($\sqrt{Hg * S}$) can provide a differentiated map of potential cinnabar presence.

An intriguing functionality within the analytical framework is the capability to identify specific color occurrences within an image. This feature facilitates operations analogous to those previously delineated, with an added emphasis on color, which bears a direct correlation to pigment composition. Given that the images under analysis serve as maps, they enable the synthesis of composite maps through the amalgamation with elemental maps. The objective is to generate maps that isolate a singular color, effectively

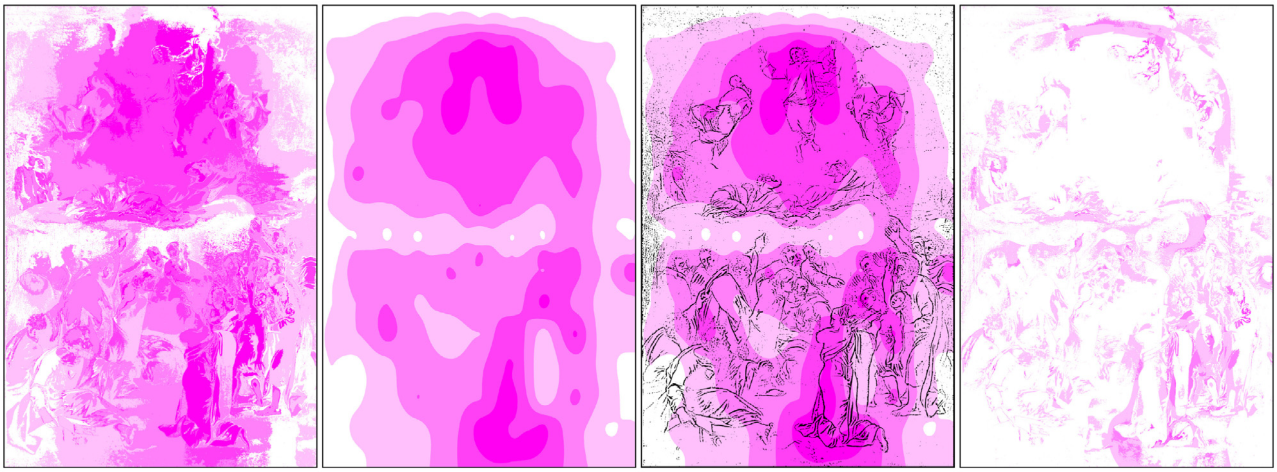

(a) Arsenic (As) MHD (b) Arsenic (As) RBF Linear (c) Arsenic (As) RBF plus contours (d) Difference between MHD and RBF

Fig. 3. An example illustrating the differences between MDH and RBF maps. The contour image helps in understanding the RBF distribution. A powerful possibility is to compare the **difference** between MDH and RBF maps, assisting experts by means of showing the the areas where the changes are greatest.

differentiating it from others. This necessitates a departure from the RGB color model, which, despite its utility in distinguishing primary colors (red, green, and blue), falls short in accurately representing color mixtures. For instance, while the RGB model readily identifies pure red (1,0,0), it is less adept at differentiating hues such as yellow (1,1,0) or orange (1, 0.6, 0.2). The resolution to this limitation lies in adopting a color model adept at nuanced color identification. In this instance, the HLS model (Hue, Lightness, Saturation) is employed. This model facilitates the distinction of fundamental colors based on hue, effectively mitigating the influence of brightness variation (black addition) and saturation variability (white addition). Having outlined the methodology in a preliminary manner, a detailed exposition of the techniques follows.

To facilitate the definition of diverse combinations, a functional language has been devised. This language operates on a premise where a set of inputs is subjected to a specific function or process, resulting in an output. Functions designed to accept one or more inputs are capable of effecting a transformation on the data, while those without inputs are configured to directly generate an output. This approach underscores the capacity to construct intricate relationships through the strategic combination of functions. Defined functions are applied at the pixel level across maps or images, culminating in the generation of a new map.

This language categorizes functions into five types:

- **Image function:** This function represents the RGB image and only has an output.
- **Element functions:** These functions represent the element maps that are produced with the interpolation methods and only have an output.
- **Conversion functions:** These functions produce a conversion of the input data to generate the output data. Two conversion functions have been defined:
  - **Binary (BIN):** Converts continuous values to a binary value: true or false. Below a threshold (selected by the user), all values become 0, and above it, they become 1, implying non-existence or existence, respectively. It takes one continuous input and produces one binary output.
  - **Color to binary (COL BIN):** This function allows searching for a specific color (selected by the user) in the original image, with a certain level of tolerance, and obtaining a binary map. It takes the color image as input and produces a binary output.
- **Logical functions:** These functions have two inputs, which must be binary, and produce one binary output. The implemented logical functions are as follows:
  - **NOT (∼):** Inverts the input; 0 becomes 1 and 1 becomes 0.
  - **AND (&):** Performs a logic AND operation. This means that a 1 is obtained only if both inputs are 1. Otherwise, the result is 0.
  - **OR (|):** Performs a logic OR operation. This means a 1 is obtained if both inputs are 1 or if either of them is one. Only if both are 0, the result is 0.
- **Numeric operations:** These functions enable operations on two elements with real values, producing real values. The function incorporates a third input, which must be a binary map, producing the effect that the function is applied only where the logical map is true: If the binary map value is true, the operation is applied and a value is produced. Otherwise the result is 0. By default, if the third input is not included, all positions are considered true. The following operations have been implemented:
  - **Element:** The result is the value of the element only where the binary map is true. For example, this function can be used to get the map where one element is present, depending on a color.
  - **Element Remove:** The result is the value of the element removing some threshold only where the binary map is true. For example, this function can be used to get part of an element, which can be useful when it is combined in several pigments.
  - **Product:** Applies the geometric mean. Given the A and B inputs it produces $\sqrt{A*B}$ as output. For example, this function can be used to get the map of a relation between two elements.
  - **Sum:** Applies the operation A+B.
  - **Difference:** Applies the operation ABS(A-B) (ABS means absolute value). For example, this function can be used to get the map with the difference of two maps produced with different interpolation methods.
  - **Percentage Sum:** Applies the operation A%+B%. This means it is performed if the values of A and B meet certain proportions. For example, to look for areas where A is twice as much as B. This can be used to simulate a chemical formula.

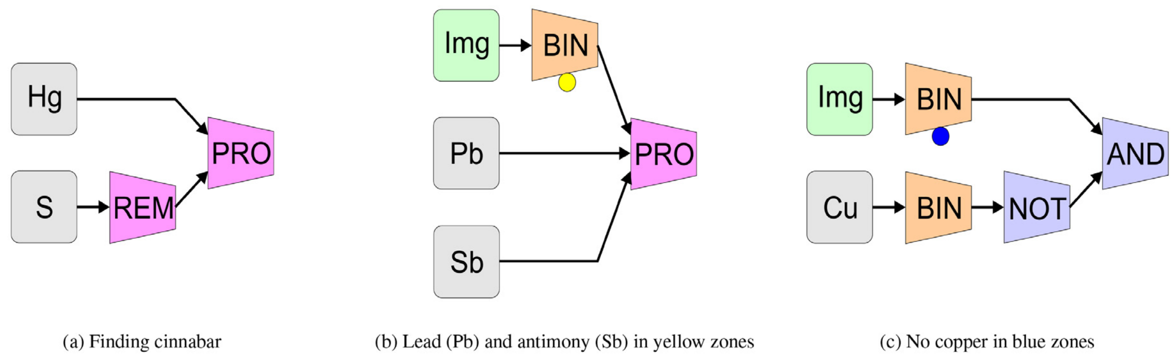

Fig. 4. Block diagrams of the various example operations. (4a) The maps of mercury (Hg) and sulfur (S) removing a threshold is firstly obtained, and then are combined with an PRODUCT operation. (4b) A binary map of the zones with yellow color is produced with the COLOR_BIN operation. A PRODUCT operation is used to combine the lead and the antimony, but controlled by the color map. (4c) A binary map of the zones with blue color is produced with the COLOR_BIN operation. A binary map of the copper is obtained with the BINARY operation. Then the result is negated with the NOT operation. Finally, the color map and the NOT map are combined with an AND operation.

The suite of implemented functions, designed for both standalone and integrative use, facilitates the empirical examination of hypotheses or specific conditions within the analytical framework. For instance, the presence or absence of a particular element within a map can be discerned through the application of a binary conversion operation followed by the negation of its results. This allows for the identification of regions devoid of the specified element. Similarly, to ascertain the coexistence of two elements, an AND operation or a multiplication can be employed, effectively isolating areas of concurrent elemental presence. Extending this logic, the presence of three distinct elements can be determined through the sequential application of two AND or multiplication operations, thereby enabling a comprehensive analysis of elemental distribution.

It is important to highlight that the functional language has been operationalized within a graphical block editor framework. This editor utilizes visual blocks to represent distinct functions and connecting lines to denote the relationships between these functions. Users are empowered to craft bespoke combinations of functions through a drag-and-drop interface, facilitating the seamless assembly of functional sequences. This approach is not only user-friendly and intuitive but also supports the iterative development of complex analytical outcomes. Furthermore, the editor maintains a history of operations, ensuring that users can trace the evolution of their analysis to comprehend the derivation of final results comprehensively.

The efficacy and user-centric design of the block editor are demonstrable through an example video, at the project web site, which showcases the Laboratory module's capabilities. Additionally, block diagrams illustrating the operational logic behind the examples discussed herein are provided in Fig. 4.

3.5. Implementation

A distinguishing feature of XMapsLab in contrast to alternatives such as *SmART_scan* is its extensive utilization of Graphics Processing Units (GPUs) to execute computational methods. This approach yields substantial enhancements in processing speed. GPUs adhere to the Single Instruction, Multiple Data (SIMD) architecture, incorporating thousands of simplified processors that concurrently execute identical operations on multiple data points. This is in stark contrast to Central Processing Units (CPUs), which are comprised of a more limited number of general-purpose processors capable of handling a broader range of complex tasks.

For example, the Nvidia RTX 4090 GPU is equipped with 16,384 simplified processors, compared to the AMD Ryzen 9 7950X CPU, which contains 16 general-purpose processors. This disparity underscores the potential for substantial speed improvements through the transition from sequential to parallel programming models, although such conversion is not universally applicable.

The exploitation of GPU capabilities, alongside the deployment of specialized hardware functionalities such as textures and Shader Storage Buffer Objects (SSBOs), allows for the efficient processing of voluminous datasets and the execution of parallel computations. These technological advancements facilitate a marked increase in computational efficiency relative to CPU-based alternatives. OpenGL and GLSL version 4.6 constitute the foundational elements of our graphics library, enabling the sophisticated rendering and processing essential for XMapsLab's operation.

4. Results

4.1. Performance analysis

The efficacy of XMapsLab's implementation was assessed using artworks previously or currently under study, for which measured data were available. It is crucial to clarify that the purpose of utilizing these examples is solely to demonstrate the potential of obtaining reliable results in real-time for high-resolution images, rather than conducting an analysis of the artworks themselves.

For this performance evaluation, two distinct paintings were selected: "The Transfiguration" and "Boceto di Pablo Veronese." "The Transfiguration," believed to be a replica from Raphael's school [26] located in the Vatican, is part of a private collection and has been subjected to restoration. Its dimensions are 63.3 cm by 93.2 cm (W $\times$ H) and the image has 3020 by 4456 pixels. It was analyzed using a grid pattern, resulting in 165 measurements. In contrast, "Boceto di Pablo Veronese" is a painting on a copper support with an oval shape, which is under ongoing study [35], yielded 29 measurements from an artwork measuring 13.5 cm by 17.5 cm (W $\times$ H) and the image has 2604 by 3268 pixels. Fig. 2 presents the original color images and measurement locations, highlighting the difference in measurement distribution across the two scenarios. Additionally, this figure illustrates the lead (Pb) maps generated via both the MHD and RBF methods, showcasing the MHD method's closer alignment with the original imagery and the RBF method's tendency towards smoother transitions.

Comparative analysis of XMapsLab and *SmART_scan* implementations focused on map generation speeds. Lacking access to the *SmART_scan* code, a CPU-based version was developed for benchmarking. Testing was conducted on a high-end PC configuration, featuring an AMD Ryzen 9 7950X CPU, 64 GB of DDR5 RAM, and an Nvidia RTX 4090 GPU with 24 GB of GDDR6X memory. It is

Table 1
Execution times for MHD method in GPU and CPU per map for three examples, in seconds. Case A has an image of 3020 pixels x 4456 pixels (W × H) and 165 measurements. Case B has an image of 2644 pixels x 3268 pixels (W × H) and 29 measurements. Case C has an image of 2608 pixels x 3684 pixels (W × H) and 52 measurements.

Method	A	B	C
MHD GPU	0.292	0.191	0.214
MHD CPU	33.596	3.583	7.747
Ratio CPU/GPU	115.054	18.759	36.200

Table 2
Execution times for the implemented methods in GPU per map for three examples, in seconds. Case A has an image of 3020 pixels x 4456 pixels (W × H) and 165 measurements. Case B has an image of 2644 pixels x 3268 pixels (W × H) and 29 measurements. Case C has an image of 2608 pixels x 3684 pixels (W × H) and 52 measurements.

Method	A	B	C
MHD	0.292	0.191	0.214
RBF (linear)	0.189	0.094	0.110

pertinent to note that performance outcomes on standard configurations may vary, generally exhibiting slower speeds.

The evaluation utilized three projects: the aforementioned paintings and "The Madonna of Foligno," which involves 52 measurements and an image size of 2068 by 3684 pixels [2]. Initial tests juxtaposed the GPU-accelerated MHD method against its CPU counterpart, with time metrics recorded for the duration required to generate and display a map (Table 1). Notably, the GPU implementation exhibited the capability to render three maps per second, even under scenarios with extensive data points and large image dimensions, significantly outperforming the CPU version which necessitated over 33 s for comparable tasks. This indicates an acceleration factor of up to 115 times by the GPU version under the test conditions. Enhancements in processing speed are anticipated to be more pronounced with larger datasets and higher resolution images, further amplified by adjusting the probe variable, which influences the pixel matrix size utilized for color averaging.

Table 2 consolidates the execution times across the tested projects, affirming the high-speed performance of the implemented methods. This efficiency enables experts to dynamically interact with the software, facilitating rapid data analysis and map generation.

4.2. Accuracy of the results

In addition to the speed and capabilities of the program in generating maps, it is essential to assess their validity and the reliability of the obtained results. It should be noted that the goal is to extract accurate information at hundreds of thousands or even millions of positions from just a few dozen or hundred measurements. In reality, zero error can only be guaranteed at the measured positions, while accuracy in the remaining positions depends on the interpolation method and various other factors, particularly the characteristics of the artwork, the pigments (expressed as colors), and their deposition.

From a statistical standpoint, Martín et al. [24] demonstrated that the MHD method can be considered reliable, but it must be accompanied by an alternative approach to verify the results. It is important to recognize the scope of statistical reliability: while a method may perform accurately in most cases, there is always the possibility that a specific case—perhaps the one under study—may fall within the small fraction of cases where the method fails. For instance, if a method is accurate 95% of the time, there remains a 5% chance that the method may not work correctly. This underscores the importance of comparing at least two methods to corroborate results, and above all, leveraging the expert's knowledge.

Based on this assertion, the program allows for a visual comparison between the results obtained using the MHD and RBF methods, enabling experts to study in greater detail the areas where the greatest discrepancies occur. Furthermore, a **Difference** operator has been incorporated into the Laboratory, which allows pixel-by-pixel comparisons between two maps (see Fig. 3d). This operator highlights areas with greater differences through color gradation, indicating the regions with more significant variations. Using this information, experts can focus their attention on the zones that exhibit the highest discrepancies. Should uncertainty persist, the only definitive solution is to perform additional real measurements.

4.3. Illustrative examples of Laboratory

The Laboratory's versatility is highlighted through three exemplary cases, demonstrating its capacity to facilitate pigment analysis in artworks:

Cinnabar identification: This hypothesis can be tested in several ways. The simplest is to obtain the binary maps where there are mercury and sulfur and combine them with an AND operation. Another possibility would be to use the PRODUCT operator. As has been proven by checking the maps, there is a gypsum base, part of the sulfur combines with calcium and another part with mercury. To check this we can eliminate part of the sulfur with the REMOVE operation, using the rest to combine with the mercury using the PRODUCT operation. Since the results are obtained in real time, the user can check the result by varying the different parameters until the searched result is obtained. The resultant maps, illustrating the areas where cinnabar might be present, are depicted in Fig. 5, with the corresponding analytical process outlined in Fig. 4a.

Naples yellow detection: Identifying Naples yellow involves isolating regions displaying a yellow hue and assessing the co-occurrence of lead (Pb) and antimony (Sb). This hypothesis can be verified by obtaining the area where the yellow color is found (with a certain level of tolerance), which controls where the PRODUCT of lead and antimony is applied. This combination generates maps that delineate areas potentially containing Naples yellow. The example images are found as additional material. The block diagram in shown in Fig. 4b.

Exclusion of copper-based pigments: The absence of copper (Cu) in areas predominantly blue or green can exclude the presence of pigments such as azurite, Egyptian blue, or malachite. This hypothesis can be verified by obtaining the area where the color blue is found (with a certain level of tolerance), combining it with the map where copper is not found, which is obtained first by obtaining the binary version and then applying the NOT operator. The example images are found as additional material. The block diagram in shown in Fig. 4c.

These examples underscore the Laboratory module's capability to support complex analyses, enabling experts to explore various hypotheses concerning pigment composition and distribution with precision and efficiency. Through iterative operations and the integration of color-based analyses, the module offers a dynamic platform for the detailed study of artworks.

5. Data capture and alignment

Although information capture is often considered a simple process, achieving high-quality results requires a more careful approach. For instance, in the case of visible information, such as color, it is a common misconception that a simple photograph taken with any device, whether a professional camera or a personal phone, will suffice. While the availability of the artwork is a limiting factor (e.g., a piece in a studio versus one engraved on an

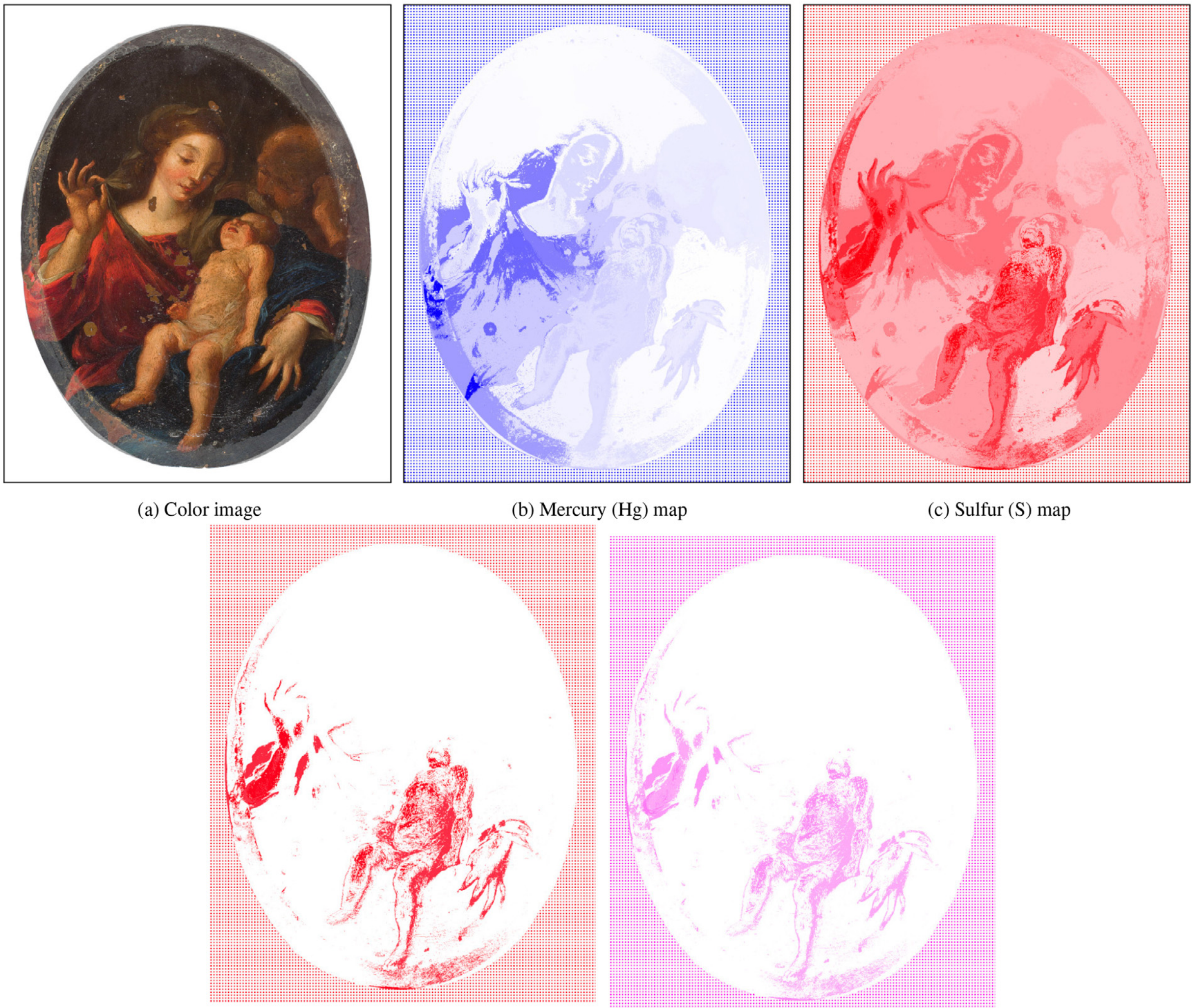

(a) Color image (b) Mercury (Hg) map (c) Sulfur (S) map

(d) The zones where there is sulfur after removing 70% of its contribution to the overall signal (e) The zones where both elements are present

Fig. 5. Operating with maps using "Boceto di Pablo Veronese": The possible presence of cinnabar can be verified by combining the areas where there is mercury (Hg) and sulfur (S). In this example, we have supposed that 70% of sulfur was combined with calcium (gypsum), leaving 30% to combine with mercury. The area with a grid indicates that there are no valid values.

outdoor monolith), it is essential to capture the information with the highest possible quality. Image size and capture format must also be taken into account. Many images are saved in JPG format to save space or for convenience, overlooking the fact that it is a lossy format. The recommendation is to take photographs in a controlled environment using a high-quality camera with distortion-free optics mounted on a tripod, under stable and uniform lighting conditions that prevent glare. Including a color reference card in some images is essential for subsequent color adjustments.

Once the best possible environment is prepared, it is crucial to control the content of the image, resolution, aspect ratio, etc., to ensure comparability with other types of images, such as X-rays. For proper comparison, the information must be aligned. If images have the same content but different sizes, rescaling can be applied. However, if their content differs, more complex image editing is required, involving rotations, translations and even deformations that introduce errors.

When generating maps from point-sampling techniques like XRF, XRD, or Raman, the visible color image often serves as a base. The visible image is used to define the map's dimensions and the positions of measured and non-measured points requiring interpolation. Proper alignment with point-sampling techniques is achieved by ensuring measurements are taken at the same positions. Failure to do so results in non-comparable values and maps, as interpolation methods are sensitive to measurement positions. If images have identical content and measurements are taken at matching positions, all results can be aligned, even if rescaling is required due to differing image sizes.

It is essential to consider the concept of sampling density, which refers to the minimum surface area over which a measurement is obtained. For images, this corresponds to the number of pixels covering a given linear space (assuming square pixels). For example, the painting "The Transfiguration" measures 63.3 cm by 93.2 cm (W $\times$ H), and its image is 3020 by 4456 pixels. This yields a sampling density of approximately 48 pixels per cm (121 pixels per inch). The area covered by a single pixel is 63.3 cm / 3020 pixels $=$ 0.02096 cm or 0.02083 cm if using the density value.

For spectrometers, the relevant parameter is the spot size, which is the diameter of the circular sampling area. For example, a ThermoFisher's Niton XL2 spectrometer has an 8 mm spot size, while the Niton XL3t has a 3 mm spot size, enabling it to capture finer details that the XL2 would miss. For XRD devices, such as the eXaminart's Duetto, the spot size is 0.8 $\times$ 0.3 mm, while the Bravo Raman spectrometer by Bruker has a spot size of ap-

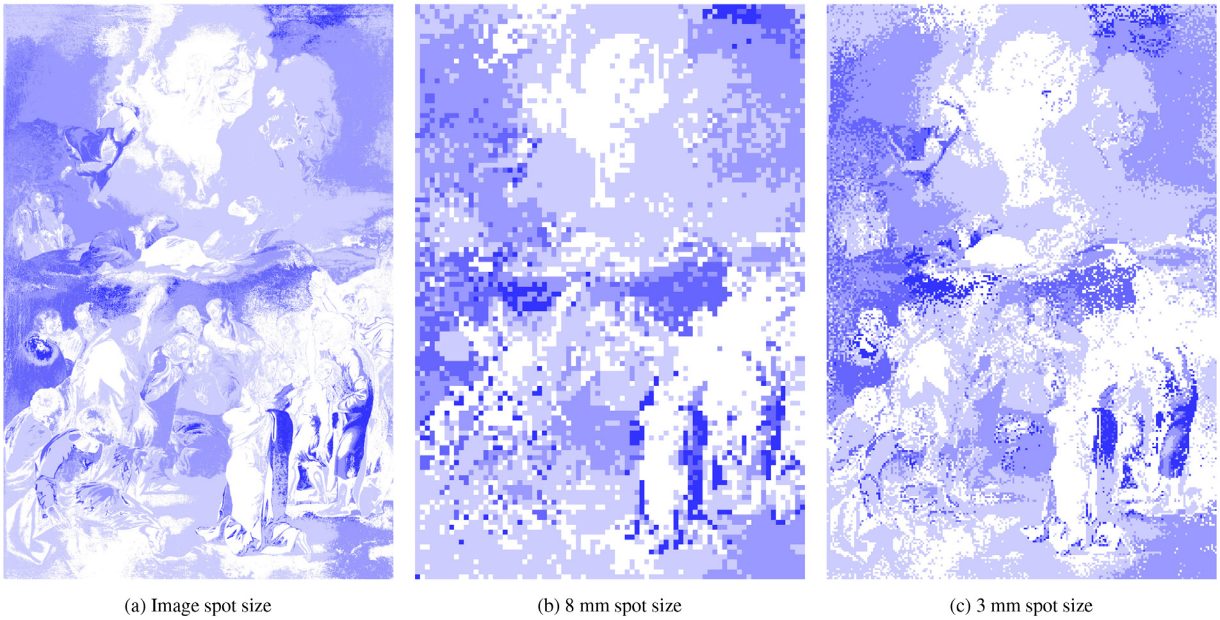

Fig. 6. Examples of interpolation maps using the spot size with "The Transfiguration" example. The MHD of potassium (K) is obtained with the virtual spot size of the color image, with a 8 mm spot size and with 3 mm spot size. The changes in the pixel density are shown in the detail of the results.

proximately 1 mm. In comparison, the equivalent pixel size for the aforementioned image would be 7.089 mm, 2.658 mm, 3.544 mm, and 0.8862 mm, respectively. Fig. 6 shows an example of the results obtained by applying the MHD method to potassium, using the virtual density of the color image, for a device with a spot size of 8 mm, and another with a spot size of 3 mm. It can be observed that as the spot size increases, the level of detail in the map decreases.

This comparison also highlights that visible images generally provide much more detail than spectrometer measurements. To correlate color images with measurements and maps obtained from them, several approaches can be used. The two methods implemented in XMapsLab prioritize either the image size or the sampling density. In the first case, assuming the image has a higher density than the measurement device, the data is treated as if it matches the image's density. This is the simplest approach. In the second case, the color image determines the map size, but calculations are performed considering the device's sampling density.

In this second case, the first step is to rescale the color image to match the sampling density. Following our example, when using the Niton XL3t spectrometer, each pixel must be adjusted from 0.2083 mm to 2.658 mm. This implies a scaling factor of 0.2083 / 2.658 = 0.078. The image size changes from 3020 by 4456 pixels to 236 by 348 pixels. Since the sampling positions are stored in a normalized format, it is straightforward to map them to the new image and perform interpolation calculations. Finally, the image must be resized back to its original dimensions using a scaling factor of 2.658 / 0.2083 = 12.8205. It is important to note that, while any rescaling method can be used for the first adjustment—linear, quadratic, or cubic interpolation being preferable—the nearest neighbor interpolation method is recommended for the second adjustment to visually highlight the effect of lower sampling density.

6. Conclusions

This paper has detailed the development and application of XMapsLab an innovative software solution tailored for the generation of detailed maps through advanced interpolation techniques. A notable advancement is the program's optimization for Graphics Processing Unit (GPU) utilization, which facilitates the processing of high-resolution images without compromising on interactive response times. This optimization is particularly beneficial for experts requiring the agility to work with extensive datasets in their analytical endeavors.

XMapsLab distinguishes itself by integrating a suite of interpolation methods alongside novel functionalities for the validation of results and the identification of pigments based on chemical element data. This suite enables the formulation of hypotheses concerning the presence or absence of specific pigments, thereby extending the analytical capabilities available to researchers.

The software is engineered to be user-centric, featuring a graphical editor that simplifies the analytical process. This design ensures that XMapsLab is accessible to a wide range of users, from those with limited technical expertise to seasoned researchers, facilitating widespread adoption within the Cultural Heritage community.

In conclusion, XMapsLab represents a significant contribution to the field of Cultural Heritage, providing a comprehensive and efficient toolset for the analysis of artworks and historical artifacts. Its development underscores the potential of combining traditional methods with cutting-edge technology to enhance the understanding and preservation of Cultural Heritage.

Availability of the program

All the resources and additional material are available at the following URLs:

- Project website: https://calipso.ugr.es/xmapslab.org
- GitHub repository: https://github.com/dmperandres/XMapsLab

Acknowledgments

This work has been funded by MCIN/AEI/10.13039/501100011033 through the project PID2020-118638RB-I00 and also by project A-HUM-164-UGR18 funded by FEDER/Junta de Andalucía - Consejería de Economía y Conocimiento. We thank the owner of "The Transfiguration" painting F. Fernández Fábregas.

References

[1] L. Musílek, T. Cechák, T. Trojek, X-ray fluorescence in investigations of cultural relics and archaeological finds, Appl. Radiat. Isot. 70 (7) (2012) 1193–1202, doi:10.1016/j.apradiso.2011.10.014.

[2] J. Daniel Martín-Ramos, A. Zafra-Gómez, J.L. Vílchez, Non-destructive pigment characterization in the painting Little Madonna of Foligno by X-ray powder diffraction, Microchem. J. 134 (2017) 343–353, doi:10.1016/j.microc.2017.07.001.

[3] M. Picollo, C. Cucci, A. Casini, L. Stefani, Hyper-spectral imaging technique in the Cultural Heritage field: new possible scenarios, Sensors 20 (10) (2020), doi:10.3390/s20102843.

[4] S. del Pozo, P. Rodríguez-Gonzálvez, L. Sánchez-Aparicio, A. Muñoz-Nieto, D. Hernandez, B. Felipe, D. González-Aguilera, Multispectral imaging in Cultural Heritage conservation, ISPRS Int. Arch. Photogramm. Remote Sens. Spatial Inf. Sci. XLII-2/W5 (2017) 155–162, doi:10.5194/isprs-archives-XLII-2-W5-155-2017.

[5] Y. Jackall, J.K. Delaney, M. Swicklik, 'Portrait of a woman with a book' : a 'newly discovered fantasy figure' by Fragonard at the National Gallery of Art, Washington, in: Burlington magazine, London, Heidelberg, 2015, pp. 248–254.

[6] F. Gabrieli, K. Dooley, J. Zeibel, J. Howe, J. Delaney, Standoff mid-infrared emissive imaging spectroscopy to identify and map materials in polychrome objects, Angew. Chem. Int. Ed. 57 (2017), doi:10.1002/anie.201710192.

[7] D. Bikiaris, S. Daniilia, S. Sotiropoulou, O. Katsimbiri, E. Pavlidou, A.P. Moutsatsou, Y. Chryssoulakis, Ochre-differentiation through micro-Raman and micro-FTIR spectroscopies: application on wall paintings at Meteora and Mount Athos, Greece, Spectrochim. Acta Part A Mol. Biomol. Spectrosc. 56 (1) (2000) 3–18, doi:10.1016/S1386-1425(99)00134-1.

[8] J. Zelinská, I. Kopecká, E. Svobodová, S. Milovská, V. Hurai, Stratigraphic EM-EDS, XRF, Raman and FT-IR analysis of multilayer paintings from the Main Altar of the st. James Church in Levoča (slovakia), J. Cult. Heritage 33 (2018) 90–99, doi:10.1016/j.culher.2018.03.006.

[9] K.H.A. Janssens, F.C.V. Adams, A. Rindy, Macroscopic X-Ray Fluorescence Analysis, Wiley, Chinchester, 2000.

[10] F.-P. Hocquet, H.-P. Garnir, A. Marchal, M. Clar, C. Oger, D. Strivay, A remote controlled XRF system for field analysis of Cultural Heritage objects, X-Ray Spectrom. 37 (4) (2008) 304–308, doi:10.1002/xrs.1076.

[11] M. Cotte, J. Susini, V.A. Solé, Y. Taniguchi, J. Chillida, E. Checroun, P. Walter, Applications of synchrotron-based micro-imaging techniques to the chemical analysis of ancient paintings, J. Anal. At. Spectrom. 23 (2008) 820–828, doi:10.1039/B801358F.

[12] G. Chiari, P. Sarrazin, M. Gaillanou, Portable XRD/XRF instrumentation for the study of works of art, Powder Difraction 8 (52) (2008) 175–186.

[13] J. Dik, K. Janssens, G. Van Der Snickt, L. van der Loeff, K. Rickers, M. Cotte, Visualization of a lost painting by Vincent van Gogh using synchrotron radiation based X-ray fluorescence elemental mapping, Anal. Chem. 80 (16) (2008) 6436–6442, doi:10.1021/ac800965g.

[14] G. Chiari, Analyzing stratigraphy with a dual XRD/XRF instrument, Powder Difraction 25 (2) (2010), doi:10.1154/1.3455001.

[15] M. Alfeld, K. Janssens, J. Dik, W. de Nolf, G. van der Snickt, Optimization of mobile scanning macro-XRF systems for the in situ investigation of historical paintings, J. Anal. At. Spectrom. 26 (2011) 899–909, doi:10.1039/C0JA00257G.

[16] K. Tsuji, T. Matsuno, Y. Takimoto, M. Yamanashi, N. Kometani, Y.C. Sasaki, T. Hasegawa, S. Kato, T. Yamada, T. Shoji, N. Kawahara, New developments of X-ray fluorescence imaging techniques in laboratory, Spectrochim. Acta Part B At. Spectrosc. 113 (2015) 43–53, doi:10.1016/j.sab.2015.09.001.

[17] D. Strivay, M. Clar, S. Rakkaa, F.-P. Hocquet, C. Defeyt, Development of a translation stage for in situ noninvasive analysis and high-resolution imaging, Appl. Phys. A 122 (2016), doi:10.1007/s00339-016-0476-y.

[18] G. Chiari, P. Sarrazin, A. Heginbotham, Non-conventional applications of a non-invasive portable X-ray diffraction/fluorescence instrument, Appl. Phys. A 11 (122) (2016) 175–186, doi:10.1007/s00339-016-0521-x.

[19] S. Kogou, G. Shahtahmassebi, A. Lucian, H. Liang, B. Shui, W. Zhang, B. Su, S. van Schaik, From remote sensing and machine learning to the history of the Silk Road: large scale material identification on wall paintings, Sci. Rep. (2020) 1–14, doi:10.1038/s41598-020-76457-9.

[20] C. Vanhoof, J.R. Bacon, U.E.A. Fittschen, L. Vincze, Atomic spectrometry update: a review of advances in X-ray fluorescence spectrometry and its special applications, J. Anal. At. Spectrom. 36 (2021) 1797–1812, doi:10.1039/D1JA90033A.

[21] S. Pérez-Diez, L.J. Fernández-Menéndez, M. Veneranda, H. Morillas, N. Prieto-Taboada, S.F.-O. de Vallejuelo, N. Bordel, A. Martellone, B. De Nigris, M. Osanna, J.M. Madariaga, M. Maguregui, Chemometrics and elemental mapping by portable LIBS to identify the impact of volcanogenic and non-volcanogenic degradation sources on the mural paintings of Pompeii, Anal. Chim. Acta 1168 (2021) http://hdl.handle.net/10810/51360.

[22] M. Vermeulen, A. McGeachy, B. Xu, H. Chopp, A. Katsaggelos, R. Meyers, M. Alfeld, M. Walton, XRFast a new software package for processing of MA-XRF datasets using machine learning, J. Anal. At. Spectrom. 37 (2022) 2130–2143, doi:10.1039/D2JA00114D.

[23] J.D. Martín-Ramos, G. Chiari, et al., SmART_scan: a method to produce composition maps using any elemental, molecular and image data, J. Cult. Heritage 39 (2019) 260–269, doi:10.1016/j.culher.2019.04.003.

[24] D. Martín, G. Arroyo, J.R. de Miras, L. López, M.R. Blanc, P. Sarrazin, J.C. Torres, Evaluation of interpolation methods for generating maps in cultural heritage chemical applications, J. Cult. Heritage 62 (2023) 293–303, doi:10.1016/j.culher.2023.06.004.

[25] D. Miriello, R. De Luca, A. Bloise, G. Niceforo, J.D. Martin-Ramos, A. Martellone, B. De Nigris, M. Osanna, G. Chiari, Pigments mapping on two mural paintings of the "house of garden" in Pompeii (Campania, Italy), Mediterr. Archaeol. Archaeom. 21 (1) (2021) 257–271, doi:10.5281/zenodo.4574643.

[26] E. Manzano, R. Blanc, J.D. Martín-Ramos, G. Chiari, P. Sarrazin, J.L. Vílchez, A combination of invasive and non-invasive techniques for the study of the palette and painting structure of a copy of Raphael's Transfiguration of Christ, Heritage Sci. 9 (2021) 899–909, doi:10.1186/s40494-021-00623-z.

[27] G. Chirco, M. de Cesare, G. Chiari, S. Maaß, M.L. Saladino, C. Martino, Archaeometric study of execution techniques of white Attic vases: the case of the Perseus crater in Agrigento, R. Soc. Chem. Adv. 12 (8) (2022) 4526–4535, doi:10.1039/D1RA06453C.

[28] G. Chirco, G. Chiari, D.F.C. Martino, Processing of XRF elementary data from the painted ceramic surface with innovative tools, J. Phys. Conf. Ser. 2204 (1) (2022), doi:10.1088/1742-6596/2204/1/012083.

[29] A. Chen, R. Jesus, M. Vilarigues, Convolutional neural network-based pure paint pigment identification using hyperspectral images, 2021, pp. 1–7, doi:10.1145/3469877.3495641.

[30] T. Kleynhans, C.M. Schmidt Patterson, K.A. Dooley, D.W. Messinger, J.K. Delaney, An alternative approach to mapping pigments in paintings with hyperspectral reflectance image cubes using artificial intelligence, Heritage Sci. 8 (84) (2020), doi:10.1186/s40494-020-00427-7.

[31] C. Jones, N.S. Daly, C. Higgitt, M.R.D. Rodrigues, Neural network-based classification of x-ray fluorescence spectra of artists' pigments: an approach leveraging a synthetic dataset created using the fundamental parameters method, Heritage Sci. 10 (88) (2022), doi:10.1186/s40494-022-00716-3.

[32] R.L. Hardy, Multiquadric equations of topography and other irregular surfaces, J. Geophys. Res. (1896-1977) 76 (8) (1971) 1905–1915, doi:10.1029/JB076i008p01905.

[33] D.G. Krige, A Statistical Approach to Some Mine Valuations and Allied Problems at the Witwatersrand, University of Witwatersrand, 1951 Ph.D. thesis.

[34] D. Marr, E. Hildreth, Theory of Edge Detection, Proc. R. Soc. B Biol. Sci. 207 (1167) (1980) 187–217 http://www.jstor.org/stable/35407.

[35] R. Blanc, E. Manzano, A. López-Montes, N. Domínguez-Gasca, J.L. Vílchez, Non-invasive study of the pigments of a painting on copper with the inscription "boceto di pablo veronese" on the back, Heritage 6 (6) (2023) 4787–4801 https://www.mdpi.com/2571-9408/6/6/254, doi:10.3390/heritage6060254.